



HAL
open science

Optimal CO₂ intake in metastable water film in mesoporous materials

Gen Li, Yong Tao, Xinping Zhu, Yining Gao, Peiliang Shen, Binbin Yin, Romain Dupuis, Katerina Ioannidou, Roland J.-M. Pellenq, Chi Sun Poon

► **To cite this version:**

Gen Li, Yong Tao, Xinping Zhu, Yining Gao, Peiliang Shen, et al.. Optimal CO₂ intake in metastable water film in mesoporous materials. *Nature Communications*, 2024, 15 (1), pp.10790. 10.1038/s41467-024-55125-w . hal-04866242

HAL Id: hal-04866242

<https://hal.science/hal-04866242v1>

Submitted on 6 Jan 2025

HAL is a multi-disciplinary open access archive for the deposit and dissemination of scientific research documents, whether they are published or not. The documents may come from teaching and research institutions in France or abroad, or from public or private research centers.

L'archive ouverte pluridisciplinaire **HAL**, est destinée au dépôt et à la diffusion de documents scientifiques de niveau recherche, publiés ou non, émanant des établissements d'enseignement et de recherche français ou étrangers, des laboratoires publics ou privés.



Distributed under a Creative Commons Attribution - NonCommercial - NoDerivatives 4.0 International License

Optimal CO₂ intake in metastable water film in mesoporous materials

Received: 21 June 2024

Accepted: 27 November 2024

Published online: 30 December 2024

 Check for updatesGen Li^{1,4}, Yong Tao^{1,4} , Xiping Zhu², Yining Gao¹, Peiliang Shen¹, Binbin Yin¹, Romain Dupuis², Katerina Ioannidou², Roland J.-M. Pellenq³  & Chi Sun Poon¹ 

The feasibility of carbon mineralization relies on the carbonation efficiency of CO₂-reactive minerals, which is largely governed by the water content and state within material mesopores. Yet, the pivotal role of confined water in regulating carbonation efficiency at the nanoscale is not well understood. Here, we show that the maximum CO₂ intake occurs at an optimal relative humidity (RH^{opt}) when capillary condensation initiates within the hydrophilic mesopores. At this transition state, the pore becomes filled with metastable low-density water, providing an ideal docking site for CO₂ adsorption and forming a mixed metastable state of water/CO₂. We prove that RH^{opt} depends on the mesopore size through a Kelvin-like relationship, which yields a robust engineering model to predict RH^{opt} for realistic mineral carbonation. Building upon classical theories of phase transition in hydrophilic mesopores, this study unveils the capacity of the metastable water in CO₂ intake and enhances the high-efficiency carbon mineralization with natural ore and industrial wastes in real-world applications.

The burgeoning global population and urbanization are escalating CO₂ emissions. The increase of atmospheric CO₂ severely exacerbates global warming and the occurrence of extreme weather¹, which places strain on sustainable development to achieve the net zero target by around 2050². Carbon capture and storage, therefore, emerges as an effective way to aid the scaling of carbon mitigation and removal efforts³, with projections indicating its full availability by 2030 and the potential to produce over 1×10^8 terajoules of energy per year by 2050⁴. Among carbon capture and storage technologies, carbon mineralization stands out⁵. It typically employs natural ores and mimics their natural carbonation process involving the accelerated reaction between CO₂ and alkaline minerals to permanently sequester CO₂ as stable carbonates (i.e., CaCO₃ and MgCO₃)^{5,6}. However, the inherently slow chemical kinetics of these reactions limit the carbonation rate, necessitating activation methods to create efficient reaction conditions⁷. Alternatively, industrial alkaline solid waste, notably

more reactive than natural resources, offers a superior carbon sink⁸. To date, millions tons of alkaline solid wastes, including iron/steel slags⁹, construction and demolition wastes¹⁰, coal fly ash¹¹, and waste gypsum¹², are disposed of through industrial recycling. Notably, cement/concrete wastes, originating from cementitious construction materials whose manufacturing process contributes to over 8.0% of total global CO₂ emission¹³, contain abundant chemically unstable components such as calcium hydroxide (Ca(OH)₂), referred to as CH that can be utilized for accelerated carbonation. These alkaline wastes exhibit enhanced carbonation reactivity in humid environments¹⁴, offering a promising avenue for accelerated carbon mineralization technology, and demonstrating a sustainable approach to harnessing industrial waste for climate change mitigation.

The feasibility of all CO₂ mineralization schemes, whether employing natural rocks or alkaline solid wastes, critically depends on carbonation efficiency, which is largely influenced by the humidity

¹Department of Civil and Environmental Engineering, and Research Centre for Resources Engineering towards Carbon Neutrality, The Hong Kong Polytechnic University, Hong Kong, China. ²Laboratoire de Mécanique et Génie Civil, CNRS and Université of Montpellier, Montpellier, France. ³Institut Européen des Membranes, CNRS and Université of Montpellier, Montpellier, France. ⁴These authors contributed equally: Gen Li, Yong Tao.

 e-mail: yong.tao@polyu.edu.hk; roland.pellenq@cnrs.fr; chi-sun.poon@polyu.edu.hk

within carbonation environments. The presence of moisture on mineral surfaces facilitates the release of cations such as Ca^{2+} through dissolution while simultaneously enabling CO_2 speciation, both of which are essential processes for promoting carbonation reactions¹⁵. Therefore, achieving efficient mineral carbonation necessitates a specific relative humidity (RH). For instance, the reaction between CH and CO_2 requires a minimum RH of approximately 8%¹⁶. Previous studies also illustrated that the thickness of water film on the CH surface determines the dissolution of CO_2 and the formation of carbonates mediated by Ca^{2+} , CO_3^{2-} , and HCO_3^- species which controls the carbon mineralization efficiency¹⁷. In large-scale engineering constructions, carbonation is diffusion-controlled since the transport of CO_2 into inner voids in between solid grains is essential for activating reactions¹⁸. The hydrophilicity of alkaline solid wastes leads to the RH-dependent water saturation states within the mesopores as described by the Kelvin equation¹⁹, which ultimately determines the overall carbonation rates of the materials. Specifically, optimal RH levels benefit the CO_2 adsorption in mesopores while a higher RH causes full saturation and hinders the channel accessibility for CO_2 transport. Experimental characterizations have been used to ascertain the water coverage in mesopores of forsterite and evaluate its effects on carbonation²⁰. A series of experiments were also conducted to validate that a favorable RH range of 50–65% accelerates the carbonation of cement pastes²¹. However, previous experimental studies have overlooked the link between the thermodynamic state of confined water and the CO_2 intake within multi-sized mesopores when seeking optimal carbonation RH. This oversight leaves the inconsistent optimal RH in different studies incomprehensible²². Atomistic simulations on calcium silicate hydrates and forsterite have demonstrated that the nanopore confinement significantly affects the domain (RH, temperature) of the stability of the adsorbed water film²³. However, the optimal states of CO_2 adsorption in confined mesopores still lack in-depth investigation.

In this study, we focus on CH, the most fundamental CO_2 -reactive mineral in alkaline solid wastes, and conduct comprehensive atomistic simulations to examine the CO_2 adsorption properties in multi-sized CH slit pores with varying water coverage (indicating different RH levels). We find that the maximum CO_2 intake occurs at the optimal RH corresponding to capillary condensation onset within the CH mesopores. This intriguing finding emphasizes the significance of transition states of confined water in activating reactions within the mesopores of hydrophilic materials. Furthermore, it enables us to establish a Kelvin-like model that accurately predicts the optimal RH for CO_2 adsorption, providing insights and guidance for accelerated mineral carbonation in practical applications.

Results

Impact of water content and state

Multiple studies have revealed that carbonation of bulk alkaline solids primarily happens in the inner mesopores with the formation of calcium carbonate reducing the porosity²⁴. Laboratory investigations further highlighted the facile mineralization reactivity occurring within a nanoconfined water film environment²⁵, where nanometer-thick interfacial water film serves as a nano-reactor for carbonation²⁰. Here, we investigate the CO_2 adsorption and diffusion behavior in mesopores ranging from 2 to 10 nm under varying RH conditions using Grand Canonical Monte Carlo (GCMC). The slit pore models, which represent the packing voids between calcium hydroxide (CH) crystal grains at the mesoscale, are employed for this analysis. It is important to note that experimental studies maintain a constant environmental RH, allowing the water exchange inside the pores to achieve dynamic equilibrium during the entire carbonation process. In our simulations, we idealize this moisture equilibration by maintaining a constant water content and not allowing water exchange throughout the CO_2 adsorption process. This approach

barely impacted the final CO_2 adsorption amount while significantly reducing computational costs.

Compared to a dry CH pore, the total CO_2 adsorption amount increases with the initial water content in the pore due to the partial CO_2 solvation in the water film (Fig. 1a–c). This observation is in line with recent experimental studies²⁶. However, it is important to note that more water does not necessarily result in better CO_2 adsorption (Fig. 1d, e). In the case of a 3 nm pore, the maximum CO_2 adsorption is observed at a water coverage of ~4 water layers (one water monolayer has a water coverage density of ~8.6 nm⁻²). A higher water coverage (43.0 nm⁻²) dramatically decreases the amount and efficiency of CO_2 adsorption due to the low diffusion coefficient of CO_2 in liquid water. The optimal water coverage density of 34.4 nm⁻² indicates a critical RH at which the capillary condensation begins (i.e., the well-defined adsorbed layered water and gaseous water suddenly fill up the entire pore as shown in Fig. 1e and Supplementary Fig. 10). The water density distribution indicates the peculiar characteristics of water at this phase transition state (Fig. 1f). The water filling the pore during capillary condensation exhibits a significantly lower density compared to normal water in the layered state, indicating a metastable state (transition state) as theorized by Saam and Cole almost 50 years ago²⁷. Based on the oscillatory mode of helium at low temperatures, they proposed a universal theory to describe the metastable state of liquids at capillary condensation within confined porous media, which later was successfully adopted by Keizer et al.²⁸ to investigate the phase transition of sulfur hexafluoride in controlled-pre glass using molecular simulations and experiments. In our simulations, we observed the CH pore appears filled with liquid water at the onset of capillary condensation, yet the actual water content is slightly lower than the theoretical volume required for complete pore filling. This incomplete filling with barely discernible air voids results in a lower average water density within the pore compared to the fully saturated state (bulk water density). For more discussion on the low-density water at capillary condensation, please consult the Supplementary Note 1. Supplementary Discussion.

The capillary condensation at the critical water content is also characterized by a sudden drop of the CO_2 diffusion coefficient within the CH channel (Fig. 1g). In the dry CH channel, the diffusion coefficients of surface-trapped CO_2 (close to CH walls) and free CO_2 (in the middle of the CH channel) are $8.0 \times 10^{-9} \text{ m}^2/\text{s}$ and $7.2 \times 10^{-8} \text{ m}^2/\text{s}$ respectively, which set the lower and upper limits for CO_2 diffusion in wet CH channels at any humidity. Gaseous CO_2 in the CH channel can be considered as freely moving gas molecules in a closed environment, but their motions are constrained by interactions with water or the solid CH surface. The red dashed lines in Fig. 1g show the attractive potential between CO_2 and CH surface (E_{att}) and the adsorption energy of CO_2 in the nanopore (E_{ads}) as a function of the water coverage density. With a coverage density of one water monolayer, the strong attractive interactions among the CH surface, CO_2 , and H_2O molecules result in the lowest CO_2 diffusion coefficient. As the water film thickness increases, E_{att} decays rapidly, causing CO_2 molecules to desorb from the CH surface to the liquid/gas interface due to the hydrophobic nature of CO_2 . This desorption leads to an increase in CO_2 diffusion coefficients. When the initial water coverage density reaches 34.4 nm⁻², the layered water film suddenly fills the entire channel and engulfs all the CO_2 in the channel (Fig. 1e). The consequent sudden drop of CO_2 diffusion coefficient indicates that this water/ CO_2 mixed state exhibits much stronger interactions than CO_2 in a layered water condition, where the high mobility of gaseous feature remains. To quantify these intensified CO_2 -water interactions with the increase in water content, we calculated the CO_2 isosteric heat of adsorption (Q_{st}) as shown in Fig. 1h. Q_{st} is defined as the negative value of the differential enthalpy of adsorption, representing the heat released per molecule added to the adsorbed phase at constant temperature and very low loadings. Therefore, a higher Q_{st} indicates greater thermodynamic stability for

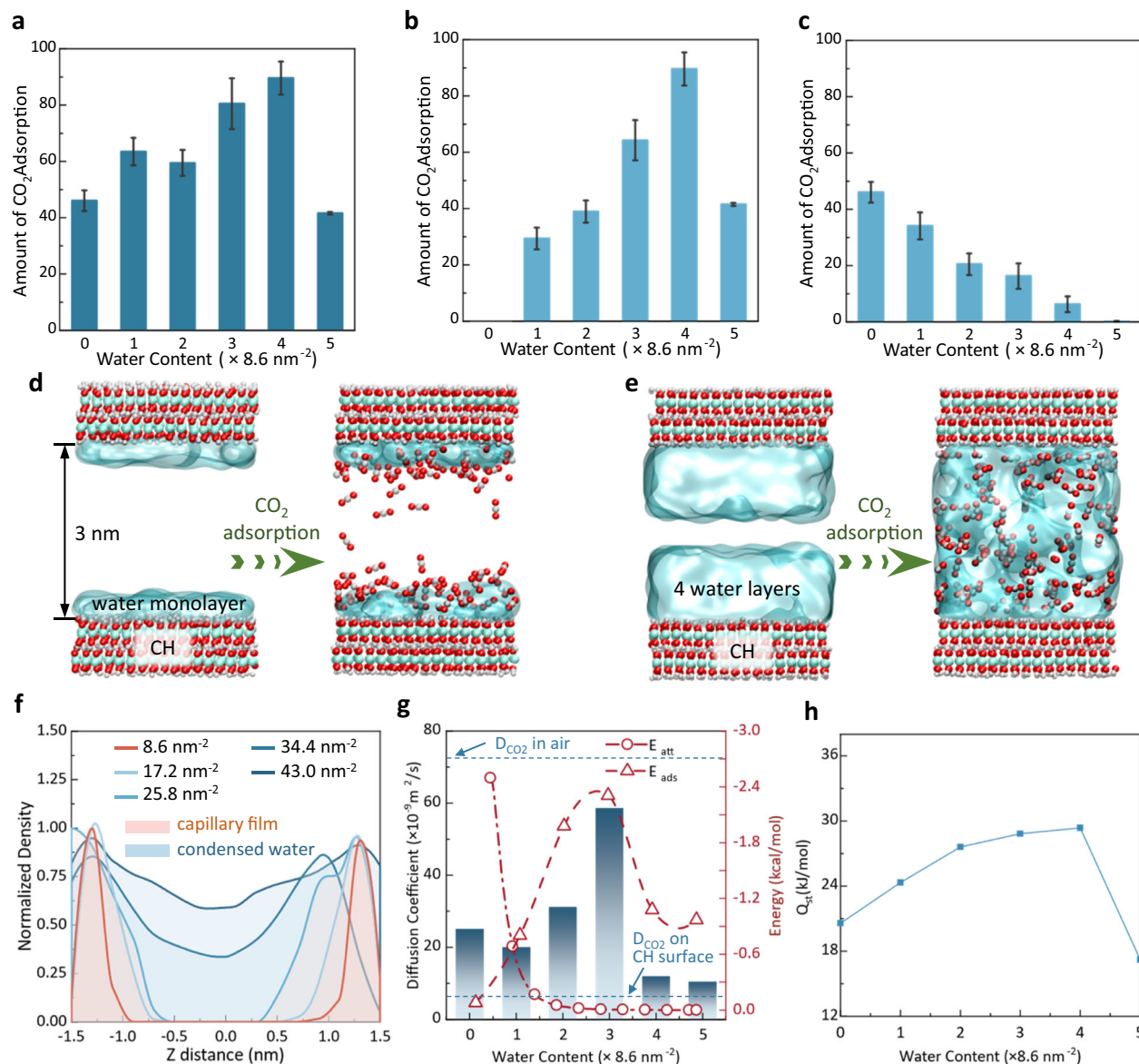


Fig. 1 | CO₂ adsorption in 3 nm CH slit pore with different water contents under 10 bars. a Total CO₂ amount in the entire channel. **b** Dissolved CO₂ amount in the interfacial water film. **c** Gaseous CO₂ amount in the CH channel. The adsorption amount is taken from the average of the last 2 ns adsorption at the equilibrium stages. The value 8.6 nm⁻² is the coverage density of one water monolayer on the CH surface. Error bars are from the standard deviation resulting from the last 1 ns simulation of CO₂ adsorption. The unit is the number of molecules. **d, e** Molecular simulation snapshots showing CO₂ adsorption into the CH channels with one and

four water layers, respectively. **f** Water density distribution along the Z direction of the CH channel at different water coverage densities. **g** Diffusion coefficients of CO₂ in the CH channel with different thicknesses of water coverage. Blue dashed lines stand for the diffusion coefficients of the surface-trapped CO₂ and free CO₂ in the dry CH nanopore. Red dashed lines designate the attractive potential between CO₂ and CH surface (E_{att}) and the adsorption energy of CO₂ (E_{ads}) as a function of the water coverage density. **h** The CO₂ isosteric heat of adsorption (Q_{st}) in 3 nm CH slit pores under varying water content. Source data are provided as a Source Data file.

CO₂ adsorption. As shown in Fig. 1h, the Q_{st} of CO₂ in CH slit pores gradually increases with water content, reaching the maximum value when water condensation occurs (water coverage density is 34.4 nm⁻²). This indicates that the CO₂-water interactions, as the driving force for CO₂ docking, are maximized at the water condensation condition, which thereby promotes CO₂ adsorption amount.

Maximum CO₂ intake

The analysis of CO₂ adsorption in a 3 nm CH channel reveals that the maximum CO₂ adsorption occurs at the RH just under which the capillary condensation jump occurs. This is further confirmed by the calculations of CO₂ maximum intake in multi-sized CH mesopores ranging from 2.0 to 10.0 nm. The dynamic CO₂ adsorption processes in

different pores over time are presented in Supplementary Fig. 2 and Supplementary Fig. 3). The CO₂ adsorption amount of the last 2 ns at equilibrium stages is analyzed and shown in Fig. 2a–f. The red boxes represent the CO₂ concentration of CH mesopores in the equilibrium state, which shows that the maximum CO₂ intake for different models all occurs at the onsite of capillary condensation. Under the maximum CO₂ adsorption conditions, the majority CO₂ molecules manifest as the dissolved state (Fig. 2g), which further confirms that the optimal CO₂ adsorption state is the metastable water/CO₂ mixed state (Fig. 1e). In addition, it is observed that the increasing pore size (2.0, 2.5, 3.0, 3.5, 4.0, 10.0 nm) requires an increasing optimal water coverage density (17.2, 25.8, 34.4, 34.4, 43.0, 111.8 nm⁻²) for maximum CO₂ adsorption, which corresponds to an increased RH. This agrees with the

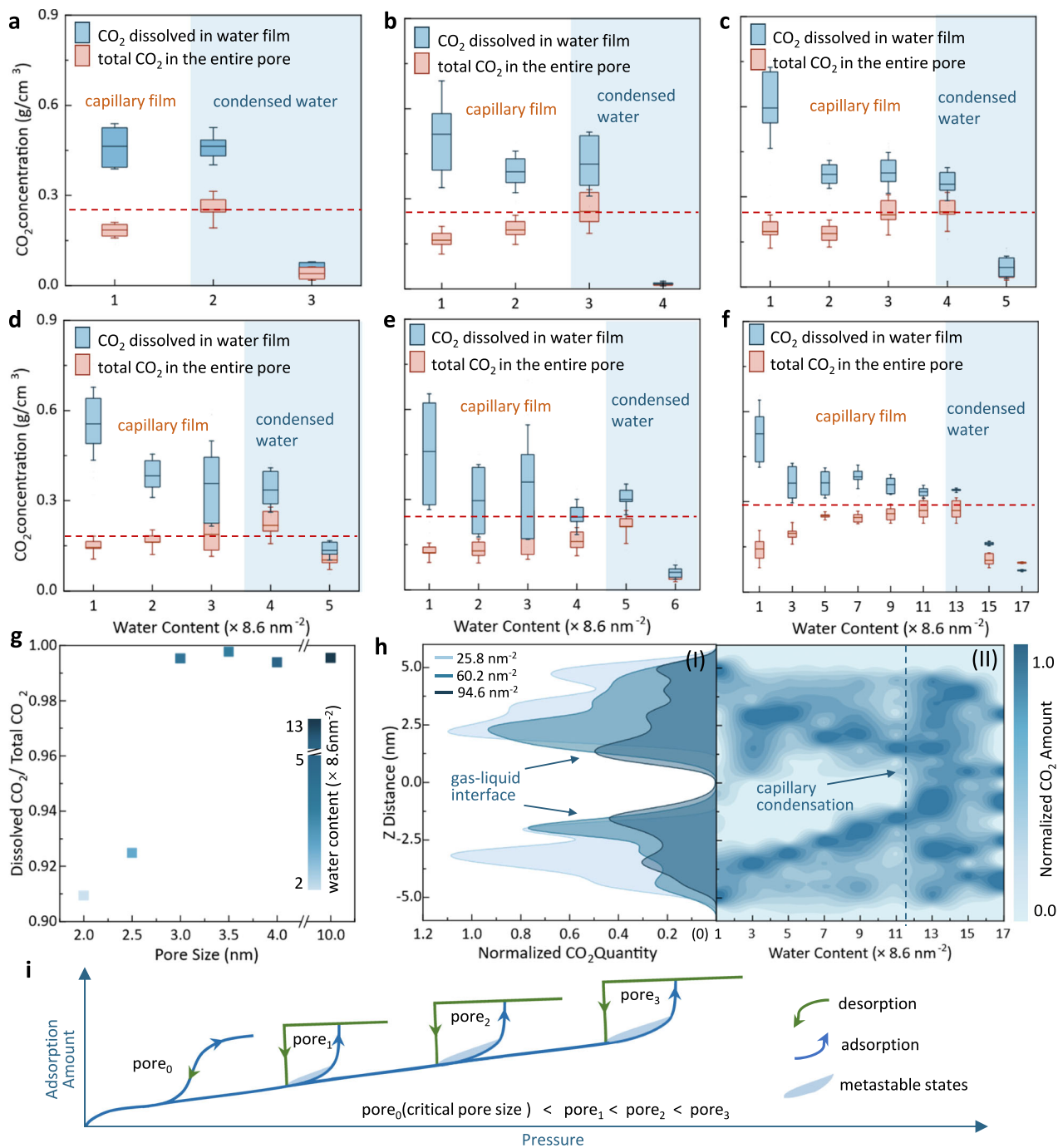


Fig. 2 | CO₂ adsorption in multi-sized CH pores with different water contents under 10 bars. a–f Equilibrium CO₂ concentrations in CH mesopores of 2.0, 2.5, 3.0, 3.5, 4.0, and 10 nm as a function of the water coverage density, respectively. The red dashed lines indicate the maximum CO₂ intake in the entire pore. Error bars are from the maximum and minimum CO₂ concentration in the last 1 ns simulation. **g** The specific values of the dissolved and total adsorbed CO₂ amount in different

CH mesopores. **h** Equilibrium CO₂ density distributions perpendicular to the 10 nm pore under different water contents: CO₂ density distributions in the channel with (I) low water contents and (II) all different water contents. **i** Schematic diagram showing hysteresis width changes of water adsorption/desorption isotherms in multi-sized mesopores. Source data are provided as a Source Data file.

dependence of condensation pressure on pore size: larger mesopores require larger water condensation pressure²⁹. The maximum CO₂ concentration in different CH mesopores exhibits a discernible threshold, which is approximately 0.28 g/cm³ and marginally varies with pore size. This critical value enlightens the maximum CO₂ adsorption capacity in CH mesopores at the current pressure. The blue boxes demote the concentration of dissolved CO₂ in water. Notably, an elevated concentration of CO₂ is observed at lower water content

(8.6 nm⁻²), which is attributed to the strong attraction exerted by the CH surface (Fig. 1g). This attractive potential decays dramatically with increasing water coverage, resulting in the decrease in CO₂ concentration to a plateau.

Before capillary condensation, CO₂ molecules accumulate at the liquid/gas boundary between the layered water and the gas space (Fig. 2h), where the dissolved and gaseous CO₂ molecules intensively exchange, reflecting the water layer instability as it is approaching the

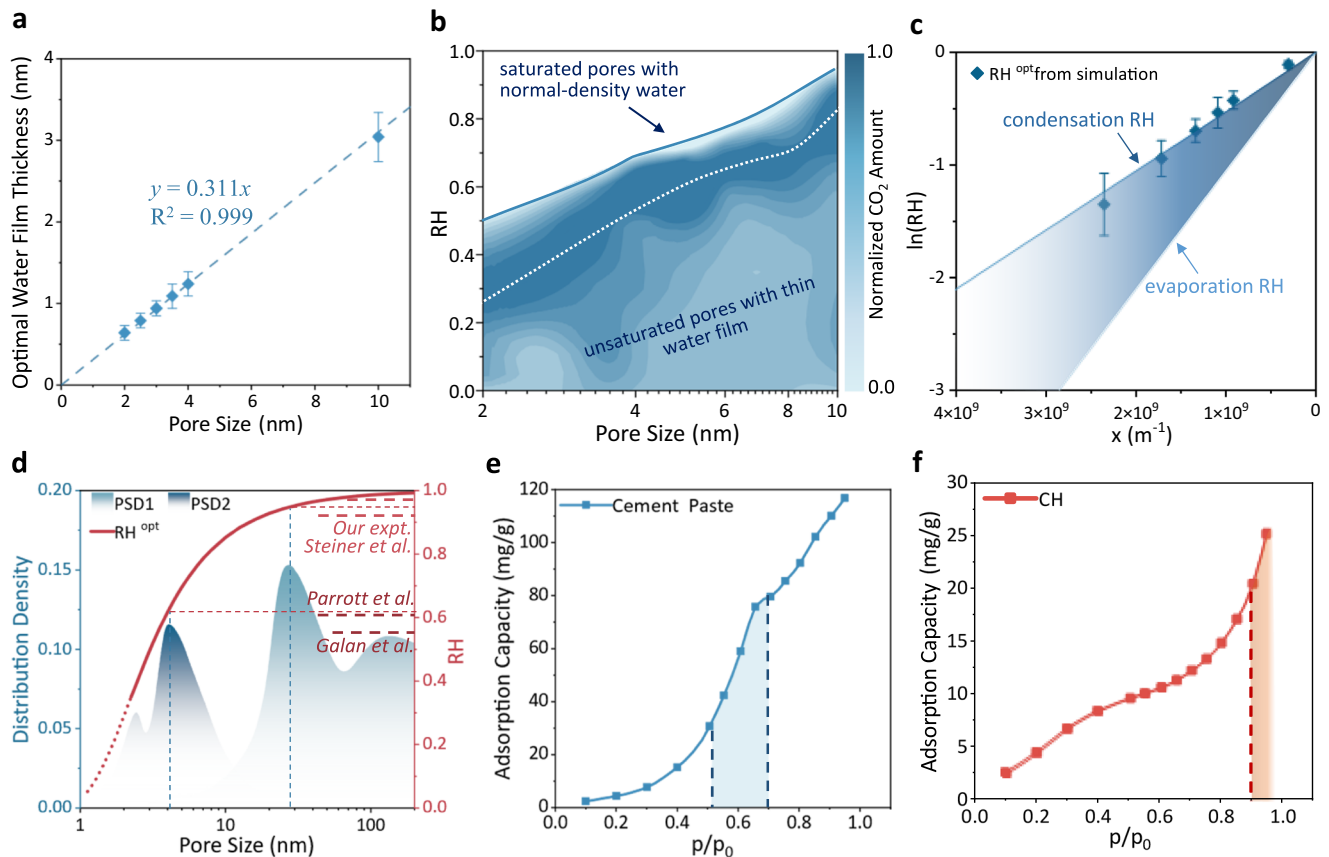


Fig. 3 | Optimal RH for CO₂ adsorption in multi-sized CH mesopores. **a** The calculated optimal water film thickness (converted from optimal water content) for CO₂ adsorption as a linear function of pore size. Error bars are from the standard deviation resulting from the fitting process. **b** CO₂ adsorption capacity as a function of RH and pore size. The amount of CO₂ adsorption is normalized to the maximum adsorption capacity for each pore size. The white dotted line denotes the optimal RH for CO₂ adsorption (RH^{opt}), where the water capillary condensation occurs in CH mesopores. **c** Evaporation RH and capillary condensation RH as a function of pore size. The capillary condensation line accurately predicts the optimal RH for CO₂ adsorption. $x = \frac{d(1-2n) + 2\delta}{d^2(1-2n)^2}$. Error bars are from the standard deviation resulting from

the fitting process. **d** Comparison of the predicted optimal carbonation RH with experimental results. The dotted line of the RH^{opt} tail indicates the pores smaller than 2 nm where the capillary condensation does not exist and the RH^{opt} model thus is invalid. The pore size distributions (PSD) of CH and cement paste have main peaks at 25 nm and 4 nm⁴⁹, respectively. The predicted RHs^{opt} is -94% and -60% respectively, which are in line with the optimal carbonation RH observed in our and previous experiments^{21,37,50}. **e**, **f** Water vapor sorption isotherms in cement paste and CH powder. The dashed lines outline the main RH (p/p_0) ranges of capillary condensation. Source data are provided as a Source Data file.

capillary phase transition. This water-layer/gas interface plays a crucial role in CO₂ adsorption and shifts toward the middle region of the CH channel as the thickness of the water film increases until capillary condensation suddenly fills the entire channel with metastable low-density water (the water liquid right after the capillary jump gets denser as RH increases), which provides an ideal CO₂ docking condition. It is important to note that the maximum CO₂ intake occurring in a domain of RH that is within the adsorption/desorption hysteresis boundaries hence corresponds to metastable pore water with large density fluctuations as described by Saam and Cole²⁷. Moreover, the hysteresis width of water adsorption/desorption isotherms increases with the mesopore size³⁰, meaning the metastable states have a broader pressure range within larger pores (Fig. 2i). This is also reflected in the CO₂ adsorption behaviors shown in Fig. 2a–f, where the 10 nm pore has a broader optimal water content range of 94.6 to 111.8 nm² compared to smaller pores.

Optimal humidity

The water contents for maximum CO₂ adsorption in different pores suggest the optimal water layer thickness, which shows a significant linear relationship with the pore size with a slope of 0.31 (Fig. 3a). It should be noted that the critical film thickness at the point of capillary

condensation (i.e., maximum water film thickness) for a slit pore is approximately 1/3 of the pore width^{31,32}, which further confirms that the optimal condition for CO₂ docking is the critical state of capillary condensation. The water content-dependent CO₂ adsorption capacity in Fig. 2a–f can be converted to an RH-dependent CO₂ adsorption capacity map for different pore sizes (Fig. 3b) through the Frenkel-Halsey-Hill equation³³. The two constants of the Frenkel-Halsey-Hill equation were determined by fitting water adsorption isotherms from our simulations and previous experiments (Supplementary Fig. 4a). It should be noted that one of the parameters α reflects the interactions between the material surface and adsorbates, which varies with respect to the material type and surface properties (details provided in the Supplementary Note 5; Supplementary Methods). Figure 3b holds engineering significance for efficient CO₂ mineralization of alkaline materials with random pore size distribution. Previous experimental studies emphasized that large pore size benefited carbon capture capacity, as the expansion of pore size consistently leads to a higher quantity of stored CO₂³⁴. However, these works tend to overlook the impact of RH and indiscriminately advocate for pore size expansion to facilitate carbon mineralization³⁵. Figure 3b suggests that achieving a comparable carbonation efficiency in small-sized nanopores is feasible by meticulously controlling the optimal RH. The white dotted line

denotes the optimal RH for CO₂ adsorption (RH^{opt}) in different CH mesopores. The regions below RH^{opt} are the unsaturated states where the pore water remains layered on the surface. Above RH^{opt} the pore is saturated with density-fluctuating metastable water, which approaches the normal-density water as RH increases. The mazarine edge line shows the upper limit of RH at which the pore is filled with normal-density water. Figure 3b shows that RH^{opt} increases with pore size: a 4 nm pore only acquires ~60% RH for maximum CO₂ adsorption, while a 10 nm pore necessitates an optimal RH of ~90%.

Since RH^{opt} indicates the capillary condensation states in the pore, it is supposed to be predicted by the Kelvin-like pore size-dependent condensation pressure, which provides valuable guidance in selecting the RH^{opt} in carbon mineralization engineering based on the pore size distribution of the materials. For hydrophilic slit pores, pore size-dependent equilibrium evaporation RH (RH^{eva}) and condensation RH (RH^{con}) respectively write:

$$\ln(\text{RH}^{\text{eva}}) = -\frac{2\gamma_0 V_m d - 2t + 2\delta}{RT (d - 2t)^2} \quad (1)$$

$$\ln(\text{RH}^{\text{con}}) = -\frac{\gamma_0 V_m d - 2t + 2\delta}{RT (d - 2t)^2} \quad (2)$$

where γ_0 , V_m , R , and T represent the planar surface tension of water, the molar volume of water, universal gas constant, and temperature, respectively. The Tolman length δ is introduced here to correct the surface tension differences between planar surface and concave meniscus³⁶. It is estimated by the water molecule size of 0.3 nm. d and t denote the pore size (diameter) and the maximum water film thickness at the capillary condensation state, respectively. The derivations of Eqs. 1 and 2 are provided in the Supplementary Note 4. Supplementary Method. Since t is proportional to d for slit pores³², letting $t = nd$, Eqs. 1 and 2 can be rewritten:

$$\ln(\text{RH}^{\text{eva}}) = kx \quad (3)$$

$$\ln(\text{RH}^{\text{con}}) = \frac{1}{2}kx \quad (4)$$

where $k = -\frac{2\gamma_0 V_m}{RT}$ is a constant of 1.05 nm at 300 K. $x = \frac{d(1-2n) + 2\delta}{d^2(1-2n)^2}$. n is approximately 1/3 yet should vary with the surface properties of the pore, which is found equal to 0.31 in our simulations (Fig. 3a). With n being determined, the theoretical RH^{con} model perfectly predicts the RH^{opt} obtained from our GCMC simulation (Fig. 3c). The deviation for the 2 nm pore is because the surface/water interaction surpasses the capillary force in small pores, making the condensation equation less valid. It is worth noting that the simulated RH^{opt} falls into the region between RH^{con} and RH^{eva} when the Tolman correction for surface tension is not taken into account (Supplementary Fig. 5). This makes general sense because RH^{con} and RH^{eva} for a finite size pore indicate the critical pressures of adsorption jump and desorption drop in Fig. 2i, respectively. The region between RH^{eva} and RH^{con} suggests the metastable saturation states of the pore, which is favorable for CO₂ intake. The incorporation of Tolman correction results in a more precise prediction of RH^{opt} that is at the onsite of capillary condensation and follows the RH^{con} line. The RH^{con} model serves as a robust model for predicting optimal RH for CO₂ sequestration with hydrophilic materials.

To validate this model, we compared the CH carbonation efficiency at different RH environments in experiments. The pore size distribution (PSD) of CH powder has a main peak at ~25 nm (Fig. 3d). Thus, the predicted RH^{opt} is ~94%, which agrees with our experiments where the samples at 98% RH were carbonated much faster than those at RHs of 10%, 30%, 55%, and 75% (Supplementary Fig. 6). Similar to our

results, Steiner et al.³⁷ also found that the carbonation of CH was much faster at 91% RH than at 57%. In addition, we examined our prediction model with another data set of cement paste carbonation experiments. The cement paste has a smaller PSD with a main peak at ~4 nm due to the porous nature of the amorphous calcium silicate hydrates. The corresponding RH^{opt} is predicted to be ~60%, which is also in line with the experimental results (Fig. 3d). Moreover, our experiments of water vapor sorption isotherms confirm that the main RH ranges of capillary condensation for cement paste and CH powder are 50–70% and >90% respectively (Fig. 3e, f), which are in line with their RH^{opt}, validating our conclusion that optimal CO₂ intake happens at the critical RH of capillary condensation. The validated model can be utilized to predict the optimal carbonation RH not only in laboratory studies but also in industrial applications. Currently, industrial activities related to carbon mineralization often rely on maintaining a constant RH, based largely on experience-based data. This approach overlooks the pore size distribution of different materials, which may deviate from the optimal conditions. Our proposed model serves as a guideline to enhance carbon capture and storage efficiency across various industrial processes, ultimately reducing labor and production costs and contributing to the achievement of net-zero emissions by 2050.

Discussion

The porous system develops in alkaline solids, wherein mesopores serve as efficient media for CO₂ docking (Fig. 4a). Mineral carbonation within mineral pores can be broadly divided into five steps: CO₂ diffusion into pores (physisorption), which reaches equilibrium rapidly; Dissolution of surface ions (release of metal and hydroxide ions); CO₂ speciation (conversion to HCO₃⁻/CO₃²⁻ in pore solution); Reaction of HCO₃⁻/CO₃²⁻ with metal ions and precipitation; Nucleation and growth of carbonation products. While the first step (physisorption) reaches equilibrium quickly, the remaining steps are non-equilibrium processes that continue until carbonation reaches its limit. This is because CO₂ chemisorption (speciation) requires overcoming a significant energy barrier (-113 kJ/mol in pure water³⁸ and -64 kJ/mol even in alkaline environments³⁹). In contrast, CO₂ diffusion encounters almost no energy barrier, resulting in a much faster rate for physisorption compared to speciation. Our study specifically investigates the impact of water content on the equilibrium CO₂ adsorption capacity (CO₂ reservoir size) within CH pores, which dictates the concentration of reactants (CO₂) available for subsequent chemical reactions, ultimately controlling the overall carbonation efficiency. The conversion of CO₂ to HCO₃⁻/CO₃²⁻ is a time-dependent, non-equilibrium process that affects the cumulative CO₂ consumption rather than the equilibrium CO₂ adsorption capacity within pores, which therefore is not our focus. Moreover, the carbonation efficiency in slit pores is influenced by numerous complex factors, which can be broadly categorized into three areas: material properties (including surface charges, surface texture, and pore size), carbonation environment (such as temperature, CO₂ pressure, and RH), and structural dynamic variations (including changes in pore solution, pore structures, and surface properties). These factors dynamically affect both CO₂ physisorption and chemisorption in porous minerals. Among these, surface properties and textures can be generally described through the interactions between the material surface and adsorbates (see Supplementary Note 4. Supplementary Methods for more details). The effects of temperature and pressure are widely recognized as having a unidirectional causal influence within suitable intervals. In contrast, significant discrepancies in optimal RH are observed across different porous systems, largely due to substantial variations in pore size distribution. Therefore, this work aims to elucidate the intricate dynamics of optimal RH for carbonation in various porous media.

RH controls the water saturation degree of the mesopores which critically governs CO₂ adsorption capacity (Fig. 4b). The most intriguing observation is that the highest CO₂ uptake occurs at the onset of

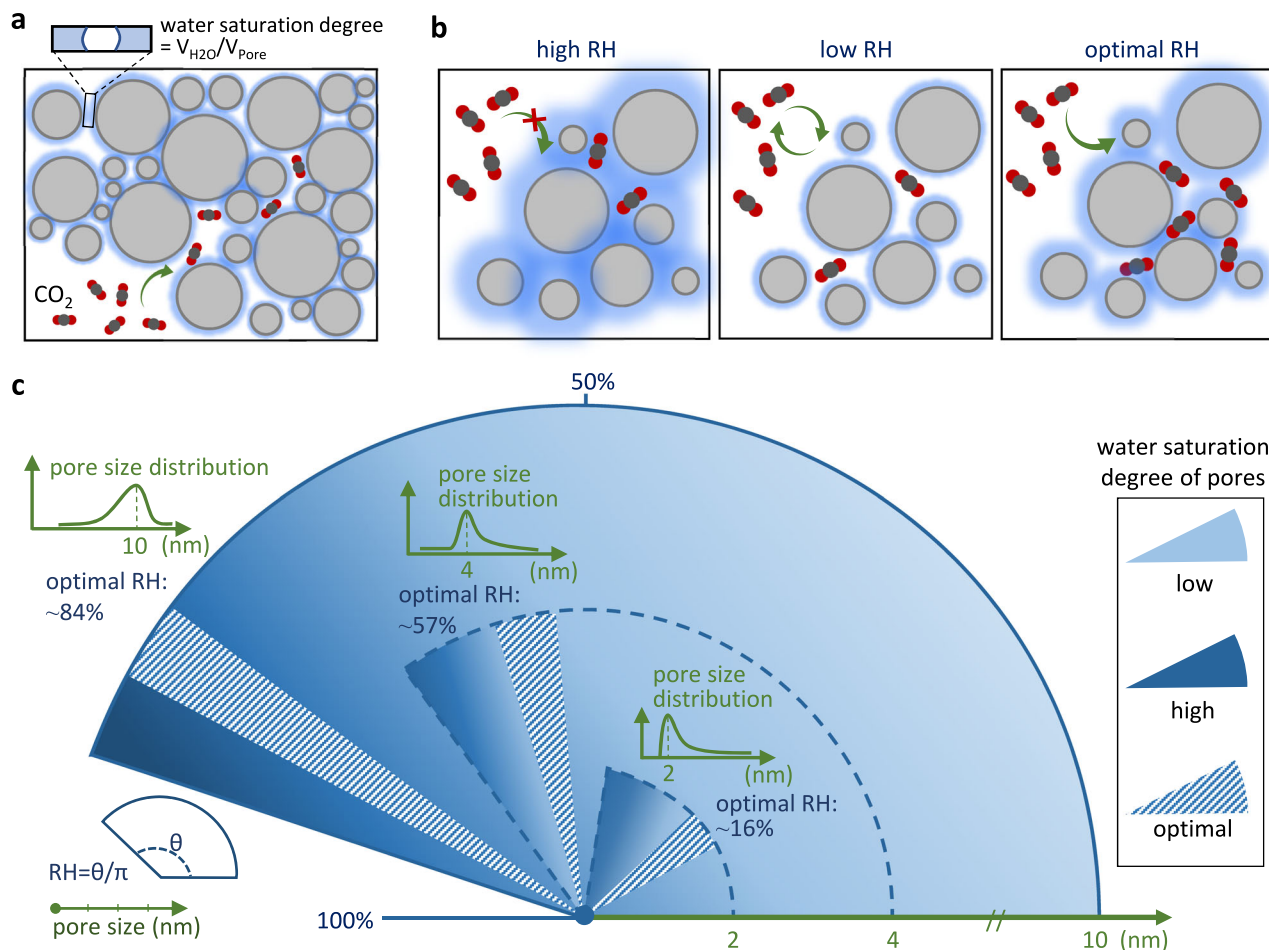


Fig. 4 | Schematic demonstration of pore size-dependent optimal RH for CO₂ mineralization. a CO₂ transport in humid mesopores. **b** The influence of RH on CO₂ adsorption in mesopores. **c** Pore size dependent optimal RH for CO₂

mineralization. When the pore size distribution (PSD) increases from 2 nm to 10 nm, the optimal RH for CO₂ mineralization (RH^{opt}) shifts from 25% to 90%.

capillary condensation, where the mesopore starts to fill with density-fluctuating metastable water, creating an ideal docking site for CO₂ adsorption. Under such circumstances, the adsorbed CO₂ exhibits “dissolved-like” states with a low diffusion coefficient but an exceptionally high concentration compared to CO₂ solubility in bulk liquid water. This observation enables us to establish the Kelvin-like relationship between the optimal RH for CO₂ adsorption and the mesopore size distribution, which is useful to predict the optimal RH for fast CO₂ mineralization in random material systems with specific pore size distribution (Fig. 4c): minerals with smaller pores achieve efficient carbonation at relatively low RH, while those with larger pores require higher RH for optimal performance. Considering that the formed calcium carbonates and other products during the carbonation process change the pore size distribution persistently, a more effective solution in experiments commences with dynamic RH^{opt} (i.e., time-dependent RH^{opt} according to the carbonation degree) to fit the pore size evolution and maximize the entire carbonation efficiency. On the other hand, to enhance the CO₂ mineralization in field experiments where the humidity control is far from trivial, our model suggests the careful control of the pore size distribution of the CO₂-reactive minerals to achieve high-efficiency carbonation. For instance, when the environment RH is 60%, the optimal carbonation efficiency will be obtained with an average pore size of ~4 nm. It is also important to note that most alkaline solids with porous structures exhibit a polydisperse pore size distribution rather than a monodisperse one, as discussed in this work. Under these realistic conditions, determining the optimal

RH becomes more complicated. From our perspective, for solids with a relatively concentrated pore distribution, the optimal RH can be selected based on the characteristics of these pore sizes. Conversely, for solids with a widely distributed pore size, a dynamically controlled RH should be employed to facilitate carbonation across different pore sizes.

Future work derived from this study will focus on two main areas. First, we aim to apply the proposed model to various mineral solids, including calcium silicate hydroxide, dicalcium silicate, and tricalcium silicate. The surface textures of these materials can significantly influence the water adsorption isotherm, which may, in turn, impact the water content required for capillary condensation. Understanding these factors is crucial for determining the optimal RH for CO₂ adsorption. The second aspect of our future work will involve extending the current model to polydisperse porous systems. We will develop a more robust model to describe the optimal RH for different porous media. Ultimately, this enhanced model will be applied in large-scale settings to improve the efficiency of industrial carbon mineralization processes.

Methods

Force field and models

In this work, the CLAYFF force field⁴⁰ is employed to describe the atomistic interactions between CH, CO₂, and water molecules. Numerous research studies have shown the capability of CLAYFF to precisely capture the solid/liquid interface behaviors in an alkaline

system^{41,42}. The incorporation of CO₂ potential in CLAYFF has been widely employed and its reliability in predicting its adsorption on wetted surfaces of clay-based materials is discussed by Cygan et al⁴³. The optimized CLAYFF force field parameters including CO₂ potentials are presented in Supplementary Table 1. It should be noted that force fields are disabled to precisely capture the CO₂ solubility in the water-rich phase and water solubility in the CO₂-rich phase under extremely high pressure^{44,45}. However, our research investigates CO₂ adsorption at a low pressure of 10 bar, where the majority of CO₂ molecules reside at the gas-liquid interface, with limited CO₂ fully dissolved in the water (although we categorized interfacial CO₂ as “dissolved CO₂” based on its coordination number with water molecules). Therefore, the accuracy of reproducing the CO₂-water phase diagram is not a critical factor in validating our simulation results.

A 2 × 3 × 4 supercell of CH molecular structure⁴⁶ was constructed and relaxed under an isobaric-isothermal ensemble at 298 K and 1 bar for 1 ns to reach full equilibrium. Then, a flat surface was obtained by cleaving the (0 0 1) surface of the CH, after which the vacuum spaces of 2 nm, 2.5 nm, 3 nm, 3.5 nm, 4 nm, and 10 nm were built to reproduce the mesopores in between CH grains. We continuously increased the water film thickness in CH slit pores by hand to mimic increasing RH until the maximum water intake was achieved. The relationship between RH and adsorbed water film thickness on the CH walls is described by the Frenkel–Halsey–Hill equation³³, the two constants of which were determined by fitting water adsorption results in experiments (Supplementary Fig. 4a and Supplementary Note 5; Supplementary Methods). The water contents and corresponding RHs are illustrated in Supplementary Table 2.

CO₂ adsorption

The adsorption of CO₂ in CH channels employed the GCMC methods⁴⁷. 100 attempts of insertion, removal, or exchange of CO₂ molecules were manipulated through GCMC methods every 1 ps, during which the CO₂ molecules were able to freely diffuse in the CH nanochannel. The whole system was relaxed under canonical NVT ensemble at 300 K during the CO₂ adsorption process to maintain stability. We employed a timestep of 1 fs for the GCMC simulation and conducted 25 million Monte Carlo moves to assess when the system could achieve full equilibrium. We found that equilibrium could be reached after 5 million Monte Carlo moves (Supplementary Note 3; Supplementary Methods). Therefore, all confined GCMC simulations were equilibrated for 5 million moves, followed by slow converging simulations for an additional 5 million steps to ensure proper convergence. The configurational-biased insertion, deletion, or reinsertion probability was set at 0.125 for CO₂, with a biased molecular translation probability of 0.375 and a maximum displacement of 0.5 Å. The biased molecular rotation probability was 0.5, with a maximum rotation of 0.05 rad. During the GCMC simulations, a canonical NVT ensemble at 300 K was employed for the equilibration of the entire system. The amount, distribution, and trajectory of adsorbed CO₂ molecules were recorded every 1 ps. The chemical potentials for CO₂ adsorption at 300 K under different pressures are shown in Supplementary Table 3. Detailed information about chemical potential is discussed in Supplementary Note 2. Supplementary Methods. All the GCMC simulations were performed in LAMMPS software.

Adsorption energy

The adsorption energy of CO₂ in the CH pore with water film was calculated through:

$$E_{\text{ads}} = E_{\text{total}} - E_{\text{CH}} - nE_{\text{CO}_2} \quad (5)$$

where E_{total} is the total potential energy of the CH slab with CO₂ adsorption. E_{CH} and E_{CO_2} are the potential energies of the CH slab with water film and a single CO₂ molecule, respectively. n is the number of

adsorbed CO₂ molecules. Specific methods for calculating E_{CH} and E_{CO_2} are presented in the Suppl. Note 1. Supplementary Methods. To record the adsorption energy variation with respect to CO₂ surface coverage, the configurations of CH with CO₂ adsorption were output every 1 ps (GCMC step). The potential energy at a certain step was then calculated through energy minimization.

Diffusion coefficient

The diffusion coefficient of CO₂ was measured by the mean squared displacement (MSD). After the CO₂ adsorption in the CH channel reached equilibrium, the system was relaxed with an NVT ensemble for another 10 ns, during which the trajectories of all atoms were recorded. Based on the trajectory data, the time-dependent $MSD(t)$ of CO₂ was calculated and the diffusion coefficient of CO₂ molecules (D_{CO_2}) was obtained by measuring the slope of MSD through the Einstein relation:

$$D_{\text{CO}_2} = \frac{1}{6} \lim_{t \rightarrow \infty} \frac{MSD(t)}{t} \quad (6)$$

Carbonation experiments

To determine the optimal RH for efficient carbonation of CH, the CH powder of analytical grade was carbonated at different RHs of 10%, 30%, 55%, 75%, and 98%. The CH samples were cured at the target RH environments (controlled by saturated solutions) with nitrogen protection gas for 5 months to ensure the inner humidity equilibrium with the environment before they were carbonated at a CO₂ pressure of 0.05 MPa for 3 h following a “semi-dry”⁴⁸ procedure. After vacuum freeze-drying for 48 h, the carbonated samples were prepared for qualitative phase analysis. The phase composition was identified by X-ray diffraction (XRD) using a Rigaku SmartLab 9 kW diffractometer with Cu K α radiation ($\lambda = 1.54 \text{ \AA}$). The scanning covered a 2θ range of 5–60° with a step size of 0.02° and a rate of 2°/min. The Rietveld method was adopted for phase quantitation with a weighted residual (Rwp) value of less than 10%. The pore structure analysis was carried out using an automatic specific surface area and porosity analyzer (Micromeritics ASAP 2020Plus). Nitrogen gas was chosen as the adsorption gas after the samples were degassed for 10 h.

Water sorption experiments

Water vapor sorption isotherms were measured gravimetrically at 20 °C using a vacuum gas/vapor sorption analyzer (BSD-VVS). The CH and cement paste samples were vacuum-dried at 60 °C for 48 h to remove residual moisture before vapor sorption. The RH (0–95%) was precisely controlled by mixing the dry argon gas with water-saturated argon flow. The sample was continuously weighed through a high-precision ($\pm 0.1 \mu\text{g}$) weighing instrument as the RH was adjusted. At each RH level, the vapor sorption continued until the weight change was less than 0.1 mg/60 min, ensuring the equilibrium of sorption at each RH.

Data availability

The data supporting the findings of this study are included within the paper and its Supplementary Information. Source data are provided with this paper.

Code availability

All the software used in this work is open source. No specific code was developed for this work.

References

1. Mysiak, J., Surminski, S., Thieken, A., Mechler, R. & Aerts, J. Brief communication: Sendai framework for disaster risk

- reduction—success or warning sign for Paris? *Nat. Hazards Earth Syst. Sci.* **16**, 2189–2193 (2016).
- Fankhauser, S. et al. The meaning of net zero and how to get it right. *Nat. Clim. Change* **12**, 15–21 (2022).
 - Pan, S.-Y. et al. CO₂ mineralization and utilization by alkaline solid wastes for potential carbon reduction. *Nat. Sustain.* **3**, 399–405 (2020).
 - Kramer, G. J. & Haigh, M. No quick switch to low-carbon energy. *Nature* **462**, 568–569, (2009).
 - Matter, J. M. et al. Rapid carbon mineralization for permanent disposal of anthropogenic carbon dioxide emissions. *Science* **352**, 1312–1314 (2016).
 - Wang, F. & Dreisinger, D. Carbon mineralization with concurrent critical metal recovery from olivine. *Proc. Natl Acad. Sci.* **119**, e2203937119 (2022).
 - Xie, H. et al. Scientific and engineering progress in CO₂ mineralization using industrial waste and natural minerals. *Engineering* **1**, 150–157 (2015).
 - Renforth, P. The negative emission potential of alkaline materials. *Nat. Commun.* **10**, 1401 (2019).
 - Pan, S.-Y., Chiang, P.-C., Chen, Y.-H., Tan, C.-S. & Chang, E. E. Ex situ CO₂ capture by carbonation of steelmaking slag coupled with metalworking wastewater in a rotating packed bed. *Environ. Sci. Technol.* **47**, 3308–3315 (2013).
 - Kaliyavaradhan, S. K., Ling, T.-C. & Mo, K. H. Valorization of waste powders from cement-concrete life cycle: a pathway to circular future. *J. Clean. Prod.* **268**, 122358 (2020).
 - Ukwattage, N. L., Ranjith, P. G., Yellishetty, M., Bui, H. H. & Xu, T. A laboratory-scale study of the aqueous mineral carbonation of coal fly ash for CO₂ sequestration. *J. Clean. Prod.* **103**, 665–674 (2015).
 - Rahmani, O. An experimental study of accelerated mineral carbonation of industrial waste red gypsum for CO₂ sequestration. *J. CO₂ Utilization* **35**, 265–271 (2020).
 - Scrivener, K. L., John, V. M. & Gartner, E. M. Eco-efficient cements: potential economically viable solutions for a low-CO₂ cement-based materials industry. *Cem. Concr. Res.* **114**, 2–26 (2018).
 - Shen, P. et al. Production of aragonite whiskers by carbonation of fine recycled concrete wastes: an alternative pathway for efficient CO₂ sequestration. *Renew. Sustain. Energy Rev.* **173**, 113079 (2023).
 - Wang, Y. et al. An integrated absorption–mineralization process for CO₂ capture and sequestration: reaction mechanism, recycling stability, and energy evaluation. *ACS Sustain. Chem. Eng.* **9**, 16577–16587 (2021).
 - Shih, S.-M., Ho, C.-S., Song, Y.-S. & Lin, J.-P. Kinetics of the reaction of Ca(OH)₂ with CO₂ at low temperature. *Ind. Eng. Chem. Res.* **38**, 1316–1322 (1999).
 - Park, J. H. et al. Role of intercalated water in calcium hydroxide interlayers for carbonation reaction. *Chem. Eng. J.* **420**, 130422 (2021).
 - Santos, R. M. et al. Stabilization of basic oxygen furnace slag by hot-stage carbonation treatment. *Chem. Eng. J.* **203**, 239–250 (2012).
 - Gelb, L. D., Gubbins, K., Radhakrishnan, R. & Sliwinski-Bartkowiak, M. Phase separation in confined systems. *Rep. Prog. Phys.* **62**, 1573 (1999).
 - Placencia-Gómez, E. et al. Critical water coverage during forsterite carbonation in thin water films: activating dissolution and mass transport. *Environ. Sci. Technol.* **54**, 6888–6899 (2020).
 - Galan, I., Andrade, C. & Castellote, M. Natural and accelerated CO₂ binding kinetics in cement paste at different relative humidities. *Cem. Concr. Res.* **49**, 21–28 (2013).
 - Drouet, E., Poyet, S., Le Bescop, P., Torrenti, J.-M. & Bourbon, X. Carbonation of hardened cement pastes: influence of temperature. *Cem. Concr. Res.* **115**, 445–459 (2019).
 - Zare, S., Uddin, K. S., Funk, A., Miller, Q. R. & Qomi, M. J. A. Nano-confinement matters in humidified CO₂ interaction with metal silicates. *Environ. Sci. Nano* **9**, 3766–3779 (2022).
 - Rodriguez-Navarro, C., Ilić, T., Ruiz-Agudo, E. & Elert, K. Carbonation mechanisms and kinetics of lime-based binders: an overview. *Cem. Concr. Res.* **173**, 107301 (2023).
 - Miller, Q. R. et al. Anomalously low activation energy of nano-confined MgCO₃ precipitation. *Chem. Commun.* **55**, 6835–6837 (2019).
 - Song, G. et al. An investigation of CO₂ adsorption kinetics on porous magnesium oxide. *Chem. Eng. J.* **283**, 175–183 (2016).
 - Saam, W. & Cole, M. W. Excitations and thermodynamics for liquid-helium films. *Phys. Rev. B* **11**, 1086 (1975).
 - de Keizer, A., Michalski, T. & Findenegg, G. H. Fluids in pores: experimental and computer simulation studies of multilayer adsorption, pore condensation and critical-point shifts. *Pure Appl. Chem.* **63**, 1495–1502 (1991).
 - Pellenq, R. J. M., Coasne, B., Denoyel, R. O. & Coussy, O. Simple phenomenological model for phase transitions in confined geometry. 2. Capillary condensation/evaporation in cylindrical mesopores. *Langmuir* **25**, 1393–1402, (2009).
 - Nakamura, M., Ohba, T., Branton, P., Kanoh, H. & Kaneko, K. Equilibration-time and pore-width dependent hysteresis of water adsorption isotherm on hydrophobic microporous carbons. *Carbon* **48**, 305–308 (2010).
 - Lin, X. et al. Changes in water vapor adsorption and water film thickness in clayey materials as a function of relative humidity. *Vadose Zone J.* **19**, e20063 (2020).
 - Tuller, M., Or, D. & Dudley, L. M. Adsorption and capillary condensation in porous media: liquid retention and interfacial configurations in angular pores. *Water Resour. Res.* **35**, 1949–1964 (1999).
 - Coasne, B., Grosman, A., Ortega, C. & Pellenq, R. in *Studies in Surface Science and Catalysis* Vol. 144 35–42 (Elsevier, 2002).
 - Huang, L. et al. Molecular insights into kerogen deformation induced by CO₂/CH₄ sorption: effect of maturity and moisture. *Energy Fuels* **33**, 4792–4805 (2019).
 - Su, H. et al. Synthesis of high-strength porous particles based on alkaline solid waste: a promising CO₂-capturing material for mine goafs. *J. Environ. Chem. Eng.* **10**, 108467 (2022).
 - Blokhuis, E. M. & Kuipers, J. Thermodynamic expressions for the Tolman length. *J. Chem. Phys.* **124**, 074701 (2006).
 - Steiner, S., Lothenbach, B., Proske, T., Borgschulte, A. & Winnefeld, F. Effect of relative humidity on the carbonation rate of portlandite, calcium silicate hydrates and ettringite. *Cement Concrete Res.* **135**, 106116 (2020).
 - Polino, D., Grifoni, E., Rousseau, R., Parrinello, M. & Glezakou, V.-A. How collective phenomena impact CO₂ reactivity and speciation in different media. *J. Phys. Chem. A* **124**, 3963–3975 (2020).
 - Wang, X., Conway, W., Burns, R., McCann, N. & Maeder, M. Comprehensive study of the hydration and dehydration reactions of carbon dioxide in aqueous solution. *J. Phys. Chem. A* **114**, 1734–1740 (2010).
 - Cygan, R. T., Liang, J.-J. & Kalinichev, A. G. Molecular models of hydroxide, oxyhydroxide, and clay phases and the development of a general force field. *J. Phys. Chem. B* **108**, 1255–1266 (2004).
 - Li, G., Yin, B., Zhang, L. & Liew, K. The hydraulic interface towards the anti-fatigue performance of fiber-calcium silicate hydrate composites under cyclic loading. *Compos. Part A: Appl. Sci. Manuf.* **171**, 107579 (2023).
 - Tao, Y., Zare, S., Wang, F. & Qomi, M. J. A. Atomistic thermodynamics and kinetics of dicalcium silicate dissolution. *Cement Concrete Res.* **157**, 106833 (2022).
 - Cygan, R. T., Romanov, V. N. & Myshakin, E. M. Molecular simulation of carbon dioxide capture by montmorillonite using an accurate and flexible force field. *J. Phys. Chem. C* **116**, 13079–13091 (2012).

44. Jiang, H., Economou, I. G. & Panagiotopoulos, A. Z. Phase equilibria of water/CO₂ and water/n-alkane mixtures from polarizable models. *J. Phys. Chem. B* **121**, 1386–1395 (2017).
45. Liu, Y., Panagiotopoulos, A. Z. & Debenedetti, P. G. Monte Carlo simulations of high-pressure phase equilibria of CO₂-H₂O mixtures. *J. Phys. Chem. B* **115**, 6629–6635 (2011).
46. Desgranges, L. et al. Hydrogen thermal motion in calcium hydroxide: Ca(OH)₂. *Acta Crystallogr. Sect. B Struct. Sci.* **49**, 812–817 (1993).
47. Pellenq, R. J.-M. et al. A realistic molecular model of cement hydrates. *Proc. Natl Acad. Sci.* **106**, 16102–16107 (2009).
48. Zajac, M., Skibsted, J., Bullerjahn, F. & Skocek, J. Semi-dry carbonation of recycled concrete paste. *J. CO₂ Util.* **63**, 102111 (2022).
49. Huang, L. et al. Using water vapour and N₂ isotherms to unveil effects of SCMs on nanopores and evaluate hydration degree. *Cem. Concr. Res.* **164**, 107042 (2023).
50. Parrott, L. J. Carbonation, moisture and empty pores. *Adv. Cem. Res.* **4**, 111–118 (1992).

Acknowledgements

C.S.P. would like to acknowledge the support of the Hong Kong Polytechnic University and the Innovation Technology Fund. Y.T.'s contributions were supported by the Start-up Fund of The Hong Kong Polytechnic University (Project ID: P0045160) and the Professor Visiting Grant from the IEM lab of the University of Montpellier. X.Z.'s contributions were supported by the MUSE/MIPS postdoctoral program of the University of Montpellier.

Author contributions

Y.T. and G.L. conceived the study, performed the simulation, and wrote the manuscript. Y.G. performed the experiments and analyzed the data. R.J.-M.P. and C.S.P. reviewed and revised the manuscript. X.Z., P.S., B.Y., R.D., and K.I. assisted with the analysis and discussion of the results. Y.T. supervised the research. All authors contributed to the final version of the manuscript.

Competing interests

The authors declare no competing interests.

Additional information

Supplementary information The online version contains supplementary material available at <https://doi.org/10.1038/s41467-024-55125-w>.

Correspondence and requests for materials should be addressed to Yong Tao, Roland J.-M. Pellenq or Chi Sun Poon.

Peer review information *Nature Communications* thanks Carlos Nieto-Draghi, Carlos Rodriguez-Navarro and the other, anonymous, reviewer(s) for their contribution to the peer review of this work. A peer review file is available.

Reprints and permissions information is available at <http://www.nature.com/reprints>

Publisher's note Springer Nature remains neutral with regard to jurisdictional claims in published maps and institutional affiliations.

Open Access This article is licensed under a Creative Commons Attribution-NonCommercial-NoDerivatives 4.0 International License, which permits any non-commercial use, sharing, distribution and reproduction in any medium or format, as long as you give appropriate credit to the original author(s) and the source, provide a link to the Creative Commons licence, and indicate if you modified the licensed material. You do not have permission under this licence to share adapted material derived from this article or parts of it. The images or other third party material in this article are included in the article's Creative Commons licence, unless indicated otherwise in a credit line to the material. If material is not included in the article's Creative Commons licence and your intended use is not permitted by statutory regulation or exceeds the permitted use, you will need to obtain permission directly from the copyright holder. To view a copy of this licence, visit <http://creativecommons.org/licenses/by-nc-nd/4.0/>.

© The Author(s) 2024